(Preprint) AAS 25-507

A GUIDANCE METHOD FOR PROXIMITY OPERATIONS AROUND A TUMBLING TARGET IN HEO

Luca Giorcelli[*], Mauro Massari[†], and Michele Maestrini[‡]

In recent years, new international programs and the increasing space debris problem have driven research on autonomous GNC algorithms. A substantial number of active spacecraft and debris now operate in highly elliptical orbits (HEOs), and future missions, such as those supporting lunar or Martian bases, will require autonomous docking capabilities, for instance, to capture resupply vehicles. In such scenarios, targets may be tumbling uncontrollably, introducing additional complexity to proximity operations. In this article, an autonomous guidance methodology is devised for this scenario. It consists in a hybrid formulation of State Dependent Riccati Equations, which increase the strategy optimality, and Sliding Mode Control, which enforces path constraints and increases the robustness of the system. The actions evaluated by the two methods are then fused to mitigate the limitations of the stand-alone methods. The algorithm is tested via a model-in-the-loop Monte Carlo analysis, with a target that mimics the rotational conditions of Envisat, but placed in a highly elliptical orbit. The results demonstrate that the devised algorithm is capable of reaching and maintaining a selected holding point around the target, matching its tumbling motion and respecting a safe approach cone, even under system uncertainties and natural disturbances.

INTRODUCTION

Autonomous proximity operations missions have been on the rise lately, with some programs aiming at achieving in-orbit servicing, assembly of bigger structures and active debris removal. For example, multiple technologies for capture and servicing with robotic arms have been presented in the European In-Space Operations and Services cluster workshop. In this kind of missions, having an autonomous and highly robust guidance method is of paramount importance to ensure a high safety level. Additionally, the relative guidance problem becomes even more difficult when trying to capture a tumbling target. This can be the case for space debris or a spacecraft that has lost its attitude control functions. According to the Spacetrack catalog, there are currently more than 200 spacecrafts (SCs) in highly elliptical orbits (HEOs), and in the future there will be even more. This orbital regime is not being studied thoroughly in the context of relative guidance, and because of the highly non-linear relative dynamics some of the state of the art methods could fail. Among those, the research recently focused mainly on three of them: Model Predictive Control (MPC), Reinforcement Learning (RL) and Sliding Mode Control (SMC). To the author's knowledge, no studies on guidance strategies for tumbling targets in HEOs have been published yet.

MPC consists of a feedback loop, where an optimal control problem (OCP) is solved and the first

[*]PhD Student, DAER, Politecnico di Milano, Via La Masa 34, 20156, Milano.
[†]Associate Professor, DAER, Politecnico di Milano, Via La Masa 34, 20156, Milano.
[‡]Assistant Professor, DAER, Politecnico di Milano, Via La Masa 34, 20156, Milano.

optimal action is sent to the control subsystem. The method is robust and provides an optimal solution, at the cost of a higher computational load.[1] To reduce this load and to avoid the convergence problems of non-linear programming problems, the OCP is usually transformed into a quadratic problem by changing the cost function and convexifying the constraints.[2,3] This means that the relative dynamical model must also be linearized. Even though there are some formulations for elliptical orbits, like Yamanaka-Ankersen,[4] Tschauner-Hempel[5] and the linearized equations of relative motion (LERM), these still introduce errors in HEOs which could compromise the performance of the guidance system. Moreover, the dynamical model can become cumbersome to integrate into the linear constraints when targeting a moving point, like in the tumbling target case.

RL applications to the guidance problem have been increasing lately. RL consists in training a neural network, the agent, to perform a given task optimally and autonomously in a real or simulated environment. In the context of proximity operations, there are studies in which the agent is used as a complete guidance block,[6–8] or as an enhancement tool for state-of-the-art methods. In the second case, some examples are adaptive gain tuning[9] or control action optimal scheduling.[10] Its main problem is the black box nature of the neural networks. This is why RL trained agents are not trusted in proximity operations tasks, where the safety level must be kept very high to avoid catastrophic collisions. However, the inclusion of path constraints in the training is easy, the agent can produce optimal trajectories and maintain a good level of robustness while remaining computationally light.

SMC is a widely used robust control method, which is known for its high robustness to uncertainties. The algorithm is composed of two parts: the sliding surface and the control function. The sliding surface is a manifold in the state space which guides the system to the target state. The control function has to make the system converge on top of the surface and to keep it sliding on top of it, ensuring the convergence to the goal. Its application as a guidance strategy has been studied in many applications, like in soft-landing[11] and proximity operations.[12] Its main problems are the sub-optimality, the hard inclusion of path constraints and chattering. However, chattering can be reduced by correctly modeling the control function.[13] Moreover, Artificial Potential Fields (APF) has been used to include path constraints in the sliding surface.[14–17] Both of these methods do not need the inclusion of the dynamical model in the guidance law, making them a good fit for an application in HEOs. Lastly, there have been some attempts to increase the optimality of the solution. An example can be the formulation of a hybrid control action by adding to the SMC contribution a second one generated by an optimal method, such as State Dependent Riccati Equations (SDRE).[18] This is another example of the flexibility of application of SMC, which can solve some of the issues of SDRE. The algorithm has been tested only in near-circular orbits. This work is taken as an inspiration for the study reported in this article.

In this paper, the goal of the mission is to reach and maintain a holding point (HP) which is fixed in the target body frame, to allow its capture with a robotic arm. The guidance problem around the tumbling target in HEO is tackled with a coupled SDRE-SMC method. The SDRE provides an optimal solution, but without taking into account path constraints, whereas SMC provides compliance with them and a higher robustness to uncertainties. The dynamics inside the SDRE are the LERM, but a correction in the control output is implemented to take into account the additional component in the target LVLH frame generated by the tumbling motion. Path constraints are included in the guidance law via a repulsive scalar potential field, which is inserted in the sliding surface of the SMC. A high-order control function is chosen to reduce the chattering in the shorter time scales. The gains of the methods are tuned to balance the outputs, making SDRE dominant under standard conditions and SMC when in close proximity to the path constraints. The approach is divided into two main phases. In the first, the chaser matches the tumbling motion while maintaining a safe distance outside an outer keep-out zone (KOZ). In the second, the chaser begins the approach towards the inner HP while staying inside an approach cone to avoid possible appendages of the target spacecraft. The results show that the designed guidance algorithm can achieve its goal in HEOs around a tumbling target.

REFERENCE FRAMES AND DYNAMICAL MODELS

Reference Frames

Two reference frames are used in this study: the Earth-Centered Inertial (ECI) and the target SC Local Vertical Local Horizontal (LVLH). The two frames are represented in Figure.1. The LVLH x-axis is aligned with the radius vector connecting Earth's center to the target spacecraft, the z-axis is perpendicular to the orbital plane and the y-axis completes the triad.

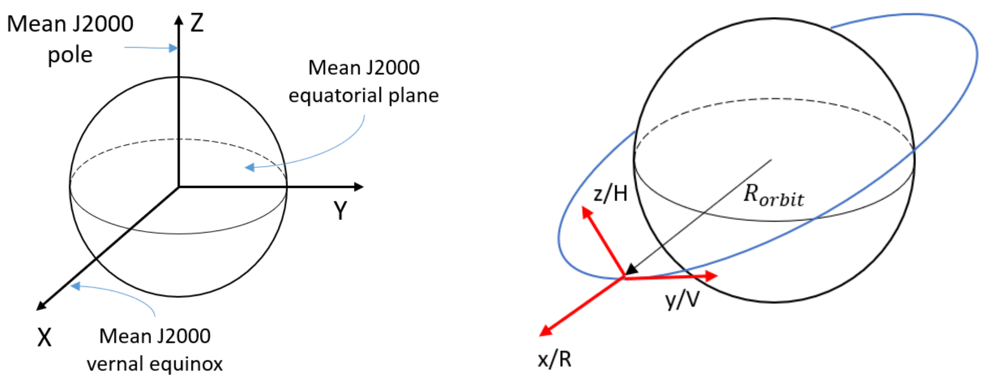

(a) ECI frame

(b) LVLH frame

Figure 1: Reference frames.

Dynamical Models

Two dynamical models are employed: the classical two body problem for the propagation of the two SCs in the simulations and the Linearized Equations of Relative Motion (LERM) inside SDRE. The two body problem equations are augmented with the J2-J5 disturbances and drag. The differential equations are formulated as in Eq.1, where $\mathbf{u}_I$ is the control action expressed in the ECI frame. The natural disturbances are taken from Reference 19 and are therefore omitted.

$$\ddot{\mathbf{r}}_I = -\frac{\mu}{r_I^3}\mathbf{r}_I + \mathbf{a}_{J2} + \mathbf{a}_{J3} + \mathbf{a}_{J4} + \mathbf{a}_{J5} + \mathbf{a}_{drag} + \mathbf{u}_I \tag{1}$$

The LERM formulation is represented in Eq.2, with $\omega, \dot{\omega}$ being the target orbital angular velocity and acceleration, h its orbital angular momentum, r_t the norm of its current orbital position and $k = \mu/h^{3/2}$. The relative state represented in the target LVLH frame is $\mathbf{x} = (r_R, r_V, r_H, v_r, v_V, v_H)$

and $\mathbf{u}$ is the control action.

$$A_{LERM} = \begin{bmatrix} 0_{3\times3} & I_{3\times3} \\ \begin{bmatrix} \omega^2 + 2k\omega^{3/2} & \dot{\omega} & 0 \\ -\dot{\omega} & \omega^2 - k\omega^{3/2} & 0 \\ 0 & 0 & -k\omega^{3/2} \end{bmatrix} & \begin{bmatrix} 0 & 2\omega & 0 \\ -2\omega & 0 & 0 \\ 0 & 0 & 0 \end{bmatrix} \end{bmatrix} \tag{2a}$$

$$B_{LERM} = \begin{bmatrix} 0_{3\times3} \\ I_{3\times3} \end{bmatrix} \tag{2b}$$

$$\dot{\mathbf{x}} = A_{LERM}\mathbf{x} + B_{LERM}\mathbf{u} \tag{2c}$$

GUIDANCE STRATEGY

The guidance strategy is divided into two main operational modes. In the first mode, or far mode, the chaser approaches an HP fixed in the body frame of the target and matches its tumbling motion, while respecting an outer KOZ. In the second mode, the chaser targets the goal HP and, when reached, tracks it for the selected amount of time. During this phase, the chaser has to respect an approach cone and an inner KOZ. The methods used in the two phases are the same, but with different gains and path constraints.

The general idea is to generate the control action as the sum of the ones obtained with SDRE and SMC.

$$\mathbf{u}_{OSMC} = \mathbf{u}_{SDRE} + \mathbf{u}_{SMC} \tag{3}$$

In the following subsections, all the vectors are expressed in the target LVLH frame unless stated otherwise.

State Dependent Riccati Equations

The formulation of SDRE is the classical one. The dynamical model of the error state $\mathbf{x}_{err}$ between the relative state of the chaser $\mathbf{x}_c$ and the current goal HP $\mathbf{x}_p$ is represented in Eq.4.

$$\mathbf{x}_{err} = \mathbf{x}_c - \mathbf{x}_p \longrightarrow \dot{\mathbf{x}}_{err} = A_{LERM}\mathbf{x}_c + B_{LERM}\mathbf{u}_1 - \dot{\mathbf{x}}_p \tag{4}$$

$\dot{\mathbf{x}}_p$ is the estimated derivative of the HP state given the tumbling motion of the target. Because of the structure needed by SDRE solvers, the system is rewritten as a ”fake” dynamical system, and a correction is applied on the control action.

$$\dot{\mathbf{x}}_{err} = A_{LERM}\mathbf{x}_{err} + B_{LERM}\mathbf{u}_{1,f} \tag{5}$$

The cost function in SDRE is the infinite horizon quadratic cost on the state error and the control, where Q and R are the gain matrices, which are different based on the mission phase.

$$J = \frac{1}{2}\int_{t_0}^{\infty} \left(\mathbf{x}_{err}^T Q \mathbf{x}_{err} + \mathbf{u}^T R \mathbf{u}\right) dt \tag{6}$$

The optimal control action can be obtained by solving the Riccati equation:

$$A_{LERM}^T P + P A_{LERM} - P B_{LERM} R^{-1} B_{LERM}^T P + Q = 0 \rightarrow P \tag{7a}$$

$$\mathbf{u}_{1,f} = -R^{-1} B_{LERM}^T P \mathbf{x}_{err} \tag{7b}$$

To solve this problem in the simulations displayed in the results section, a MATLAB built-in generalized Shur decomposition method is used. The HP is fixed in the target body frame, and so the term coming from the LERM in Eq.5 has to be canceled and replaced by its estimated acceleration, as in Eq.8.

$$\mathbf{u}_{SDRE} = \mathbf{u}_{1,f} + B_{LERM}^T \mathbf{a}_p - B_{LERM}^T A_{LERM} \mathbf{x}_p \tag{8}$$

Sliding Mode Control

The SMC must enforce path constraints and increase the robustness of the guidance algorithm. The design consists of two steps: the formulation of the sliding surface and of the control function. The sliding surface has a positional and a velocity term, and is reported in Eq.9.

$$\boldsymbol{\sigma} = \mathbf{v}_c + K_r \nabla U_r \tag{9}$$

$\mathbf{v}_c$ is the relative velocity of the chaser, K_r is the surface gain matrix and ∇U_r is the gradient in the relative position of a scalar repulsive field, which represents the path constraints. This field is different in the two operating modes. In the first mode, the only constraint is an outer KOZ.

$$U_{r,1} = 30\, e^{-\dfrac{\mathbf{r}_c \cdot \mathbf{r}_c}{200}} \rightarrow \nabla U_{r,1} = -2 \frac{\mathbf{r}_c}{200} 30\, e^{-\dfrac{\mathbf{r}_c \cdot \mathbf{r}_c}{200}} \tag{10}$$

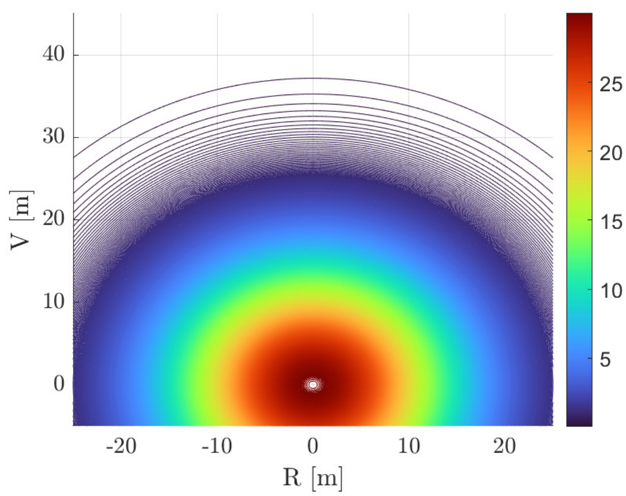

Figure 2: Outer KOZ field in the LVLH frame

In the second mode, the field contains both an inner KOZ, which represents the bulk of the target, and an approach cone. The inner KOZ is formulated like the outer one, but with different coefficients:

$$U_{r,2} = 10^3\, e^{-\mathbf{r}_c \cdot \mathbf{r}_c} \rightarrow \nabla U_{r,2} = -10^3\; 2\mathbf{r}_c\, e^{-\mathbf{r}_c \cdot \mathbf{r}_c} \tag{11}$$

The approach cone is designed to have its axis along the minus y-axis of the target body frame, an aperture angle α of 25 degrees and the vertex in $(0, 5, 0)_{t,body}$ $[m]$. The axis and vertex are then rotated in the LVLH frame ($\mathbf{a}_{cone}, \mathbf{v}_{cone}$) and the cone is formulated as in Eq.12.

$$C = (\mathbf{r}_c - \mathbf{v}_{cone}) \cdot \mathbf{a}_{cone} - cos(\alpha)||\mathbf{r}_c - \mathbf{v}_{cone}|| \tag{12a}$$

$$\nabla C = \mathbf{a}_{cone} - cos(\alpha)\frac{\mathbf{r}_c - \mathbf{v}_{cone}}{||\mathbf{r}_c - \mathbf{v}_{cone}||} \tag{12b}$$

The repulsive field is then:

$$U_{r,3} = \frac{1}{2}10^{-4}\frac{\mathbf{r}_{err} \cdot \mathbf{r}_{err}}{10^{-5}C^2} \rightarrow \nabla U_{r,3} = 10^{-4}\left(\frac{\mathbf{r}_{err}}{10^{-5}C^2} - \frac{\mathbf{r}_{err} \cdot \mathbf{r}_{err}\nabla C}{10^{-5}C^3}\right) \tag{13}$$

The total field is represented in Figure.3 and the total gradient inserted into the surface is just $\nabla U_{r,2} + \nabla U_{r,3}$.

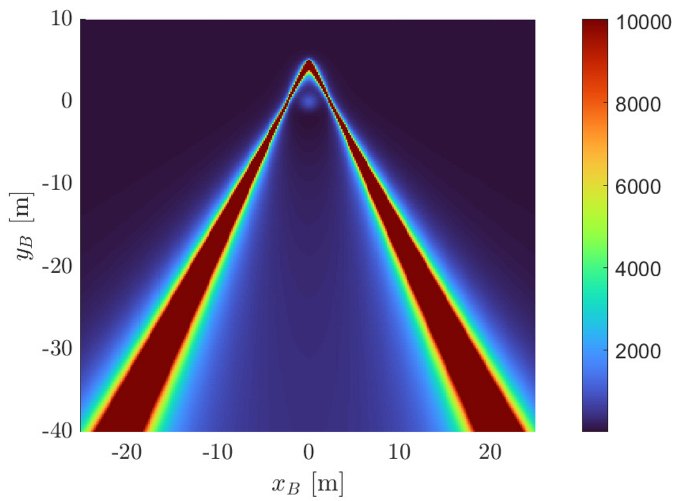

Figure 3: Repulsive field with the inner KOZ and the cone represented in the target body frame. The goal HP in $(0, -1, 0)\,[m]$. The high values of the cone constraint are saturated at 10^4 for a better representation.

The second step in the definition of the SMC is the choice of the control function. In the case at hand, in which a continuous control is considered, a high-order control law is chosen, and it is reported in Eq.14.

$$\mathbf{u}_{SMC} = -a\,|\boldsymbol{\sigma}|^{\zeta}\,tanh(\boldsymbol{\sigma}) \tag{14}$$

The values of the constants a and ζ change based on the mission phase, and are reported in the simulations section.

The switch from the first mode to the second is performed when the components of the position error are below $5\ [m]$ and the ones of the velocity error are below $0.1\ [m/s]$ Lastly, when the norms of the positional and velocity errors with respect to the inner HP are below $0.5\,[m]$ and $0.1\,[m/s]$ respectively, only the control action of SDRE is applied in order to reduce the propellant consumption during tracking.

SIMULATIONS AND RESULTS

The algorithm is tested through a MIL Monte Carlo (MC) analysis, running in closed loop at 2 Hz. The mission is divided into phases: the first two target the outer and inner HPs, whereas during the last one the chaser tracks the latter for 500 seconds. The outer and inner HPs are selected to be $(0, -35, 0)$ $[m]$ and $(0, -1, 0)$ $[m]$ in the target body frame, respectively. The tracking time is set to start when the estimated range with respect to the inner HP is below 1 $[m]$.

The SCs are placed in a Geostationary transfer orbit (GTO), and their specifics are reported in Table 1. Three different MC simulations are performed, each consisting of 100 runs, changing the orbital positions: the perigee, apogee, and at 90 degrees of true anomaly. The initial orbital configurations are fixed for all simulations in each of the cases and are represented in Table 2. The rotational state of the target is randomly selected for the quaternion part, while the rotational velocity is fixed to that of ENVISAT, which is $(0.0003, 0.0252, -0.0145)$ $[rad/s]$ in the target body frame. This should ensure that most of the possible initial relative conditions are considered in the analysis.

Table 1: SCs initial mass, face area, drag coefficient, specific impulse and thrust

m_0 $[kg]$	Face area $[m^2]$	C_D $[-]$	I_{sp} $[s]$	T $[N]$
1000	1	2	295	50

All runs are considered successful, meaning that the KOZs and the cone were not breached, and the tracking phase was reached in a limited amount of time.

Table 2: Initial orbital configuration of the two spacecrafts

Spacecraft	a $[km]$	e $[-]$	i $[deg]$	Ω $[deg]$	ω $[deg]$	θ $[deg]$
Target	24396.15	0.7283	0	0	178	$0, 90, 180$
Chaser	24396.15	0.7283	$0 + 0.0007$	0	178	$(0, 90) - 0.0004$ $180 - 0.0002$

The guidance parameters used during the tests are reported in Table 3. Those parameters have been found through a trial and error approach, considering the needed balance of dominance between the positional and velocity errors in the various mission phases.

Table 3: Guidance law parameters in the two operating modes

Parameter	Far Mode	Final approach Mode
Q	$\begin{bmatrix} 10^{-2}\, I_{3\times3} & 0_{3\times3} \\ 0_{3\times3} & I_{3\times3} \end{bmatrix}$	$r_{err} > 2\,[m] \;\rightarrow\; \begin{bmatrix} 10^{-2}\, I_{3\times3} & 0_{3\times3} \\ 0_{3\times3} & 100\, I_{3\times3} \end{bmatrix}$ $r_{err} \leq 2\,[m] \;\rightarrow\; \begin{bmatrix} 50\, I_{3\times3} & 0_{3\times3} \\ 0_{3\times3} & 10^{-1}\, I_{3\times3} \end{bmatrix}$
R	$50\, I_{3\times3}$	$50\, I_{3\times3}$
K_r	$0.5\, I_{3\times3}$	$I_{3\times3}$
a	50	10^{-2}
ζ	1	$1/1.5$

Uncertainties on the chaser navigation and propulsion subsystems are taken into account and are reported in Table 4.

Table 4: System uncertainties

Parameter	Value
Thrust misalignment	$0.03°$
Thrust	$bias = 0.02\,T, \quad wn = 0.005\,T$
Relative position	$bias = 0.05\,r_c, \quad wn = 0.01\,r_c$
Relative velocity	$bias = 0.05\,\mathbf{v}_c, \quad wn = 0.01\,v_c$

As can be seen in Figure 4, the tracking precision does not change under different orbital conditions. This means that the performance is the same even at the pericenter, where the relative dynamics are faster. Additionally, the error is of the same magnitude as the estimated state uncertainties, which means that they are its driving factor. Additional simulations were performed at different inclinations for completeness, obtaining comparable results, some of which are reported in Figure 5.

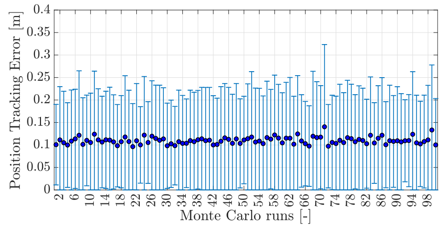

(a) Position (Pericenter)

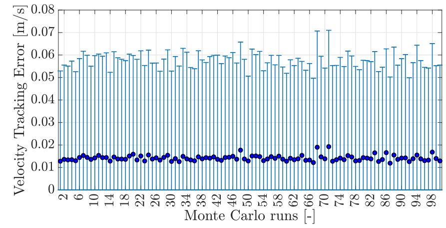

(b) Velocity (Pericenter)

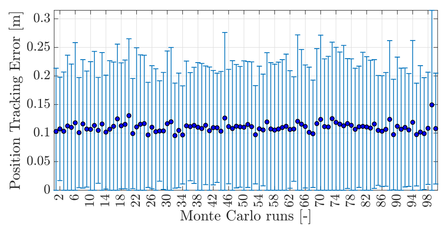

(c) Position ($\theta = 90°$)

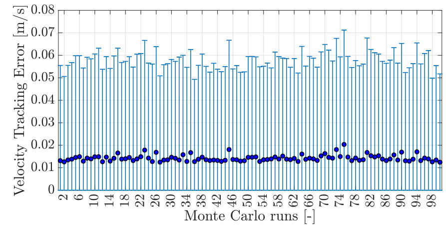

(d) Velocity ($\theta = 90°$)

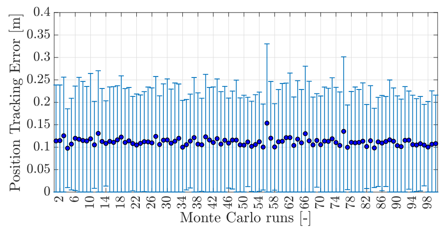

(e) Position (Apocenter)

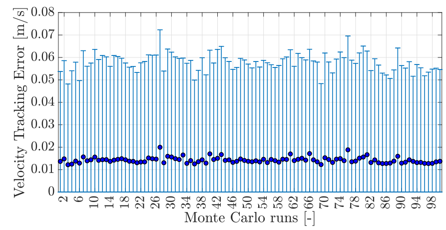

(f) Velocity (Apocenter)

Figure 4: Mean tracking errors and their standard deviations throughout the MC analysis.

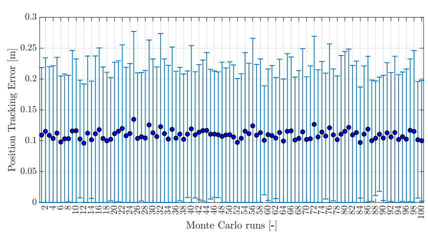

(a) Position ($i = 45°$)

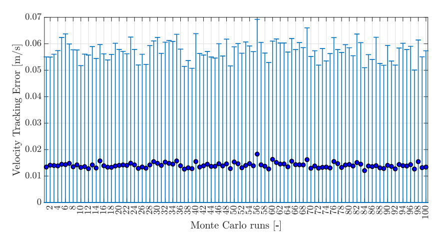

(b) Velocity ($i = 45°$)

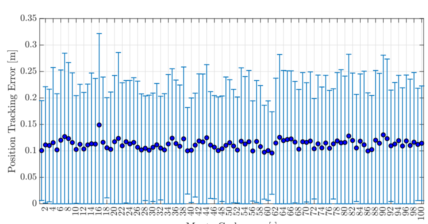

(c) Position ($i = 90°$)

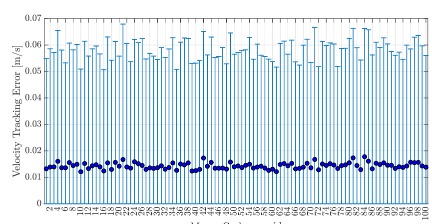

(d) Velocity ($i = 90°$)

Figure 5: Mean tracking errors and their standard deviations with different orbital inclinations ($\theta = 90°$). The results match the values obtained in the standard GTO.

In Figure 6, it can be seen that the algorithm is able to navigate around the outer KOZ and reach the HP even when it is on its opposite side. Additionally, a second behavior is visible in the zoomed plots: the initial part of the tracking phase is used to slow the approach and match the rotational motion of the goal HP while avoiding the inner KOZ.

In Figure 7 the evolution of the error state and the control action of the trajectories shown in Figure 6 are represented. The control is quite disturbed by the uncertainties on the relative state, generating chattering. An example of the control action without uncertainties is represented in Figure 8.

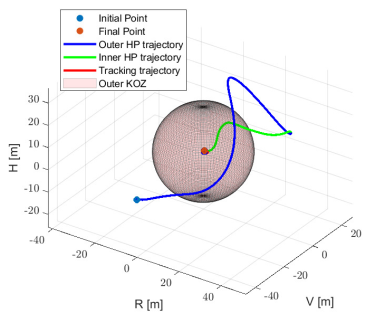

(a) Full trajectory (Pericenter)

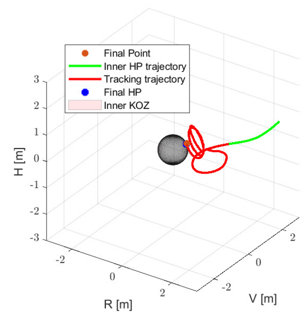

(b) Zoom on the tracking phase (Pericenter)

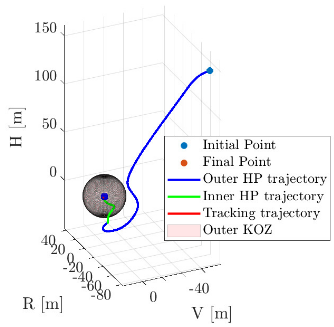

(c) Full trajectory ($\theta = 90^{\circ}$)

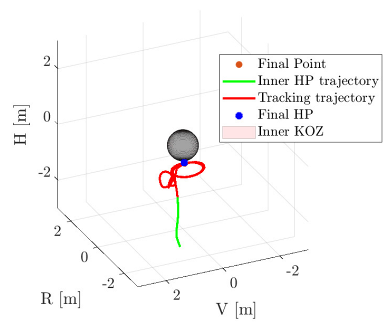

(d) Zoom on the tracking phase ($\theta = 90^{\circ}$)

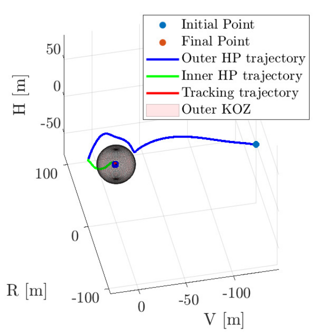

(e) Full trajectory (Apocenter)

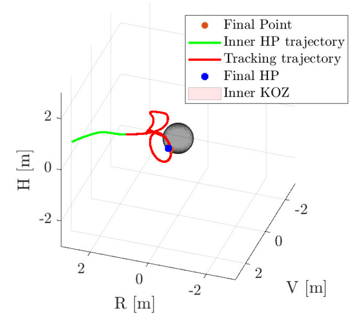

(f) Zoom on the tracking phase (Apocenter)

Figure 6: Example trajectory in the different orbital cases

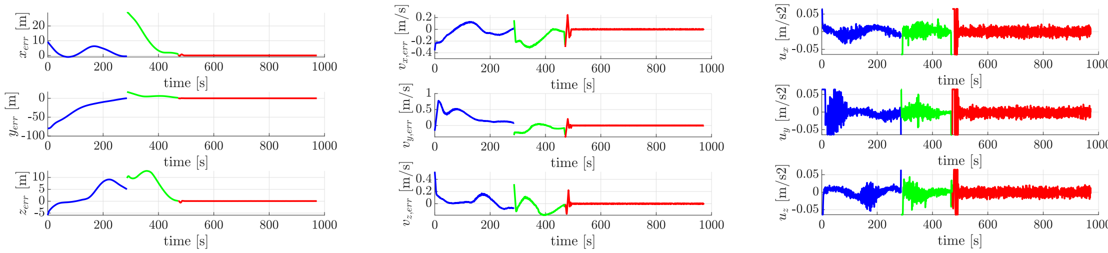

(a) Position error (Pericenter) (b) Velocity error (Pericenter) (c) Control (Pericenter)

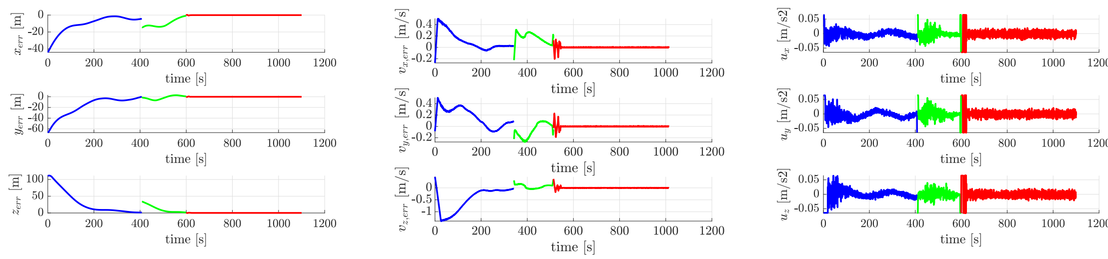

(d) Position error ($\theta = 90°$) (e) Velocity error ($\theta = 90°$) (f) Control ($\theta = 90°$)

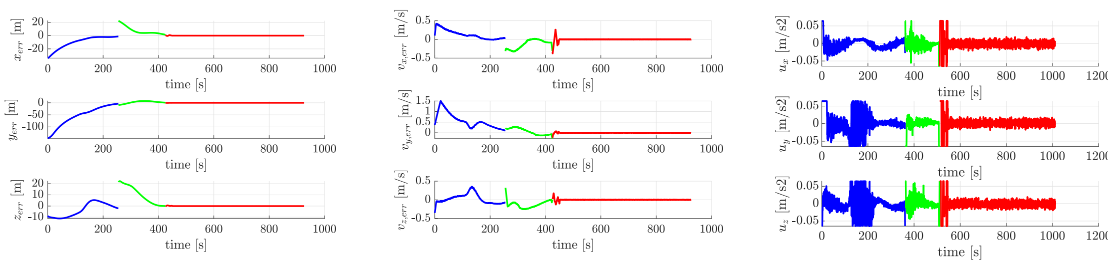

(g) Position error (Apocenter) (h) Velocity error (Apocenter) (i) Control (Apocenter)

Figure 7: Full state error and control evolution during the trajectories, same color scheme used in Figure.6

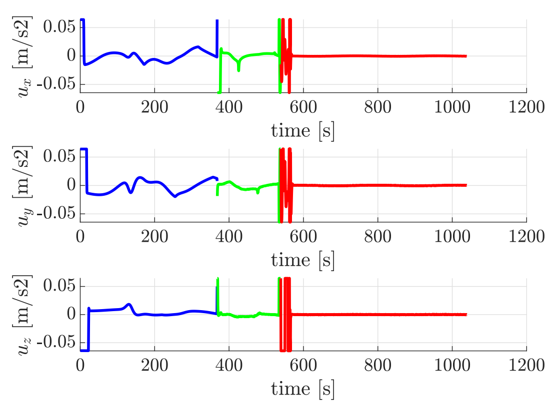

Figure 8: Control action without uncertainties, no chattering

CONCLUSIONS

Future planned missions are expected to increase the number of space objects flying in highly elliptical orbits. Those objects might lose their attitude control capabilities and begin tumbling, requiring servicing missions to recover their rotational state. In such scenarios, a servicer equipped with an autonomous guidance system will be of paramount importance. This paper presents an SDRE-SMC hybrid guidance algorithm designed for proximity operations around a tumbling target in HEOs. The mission is structured into three phases: an initial approach to a distant HP, the approach to the target HP and the tracking phase. The algorithm used throughout these phases is the same, but with different gains and active constraints. The proposed guidance scheme was tested through a Monte Carlo simulation with the target placed in a GTO, considering different initial orbital positions and tumbling states. The results show that the chaser reliably reaches the goal HP in limited time, adheres to path constraints, and maintains a low tracking error, even in the presence of system uncertainties and unmodeled natural disturbances.

ACKNOWLEDGMENT

This work is part of the Horizon Europe 2023 GEORyder project, grant agreement 101135095. The authors would like to acknowledge the support received by the European Union.

Funded by the European Union

REFERENCES

[1] A. Botelho, B. Parreira, P. N. Rosa, and J. M. Lemos, *Predictive Control for Spacecraft Rendezvous*. Springer, 2021.

[2] A. Weiss, M. Baldwin, R. S. Erwin, and I. Kolmanovsky, "Model predictive control for spacecraft rendezvous and docking: Strategies for handling constraints and case studies," *IEEE Transactions on Control Systems Technology*, Vol. 23, 7 2015, pp. 1638–1647, 10.1109/TCST.2014.2379639.

[3] X. Wang, Y. Li, X. Zhang, R. Zhang, and D. Yang, "Model predictive control for close-proximity maneuvering of spacecraft with adaptive convexification of collision avoidance constraints," *Advances in Space Research*, Vol. 71, 1 2023, pp. 477–491, 10.1016/j.asr.2022.08.089.

[4] K. Yamanaka and F. Ankersen, "New state transition matrix for relative motion on an arbitrary elliptical orbit," *Journal of Guidance, Control, and Dynamics*, Vol. 25, 2002, pp. 60–66, 10.2514/2.4875.

[5] Z. Dang, "Solutions of tschauner-hempel equations," *Journal of Guidance, Control, and Dynamics*, Vol. 40, 11 2017, pp. 2953–2957, 10.2514/1.G002774.

[6] G. Fereoli, H. Schaub, and P. D. Lizia, "Meta-Reinforcement Learning for Spacecraft Proximity Operations Guidance and Control in Cislunar Space," *Journal of Spacecraft and Rockets*, 10 2024, pp. 1–13, 10.2514/1.A36100.

[7] B. Gaudet, R. Linares, and R. Furfaro, "Six degree-of-freedom body-fixed hovering over unmapped asteroids via LIDAR altimetry and reinforcement meta-learning," *Acta Astronautica*, Vol. 172, Elsevier Ltd, 7 2020, pp. 90–99, 10.1016/j.actaastro.2020.03.026.

[8] K. Hovell and S. Ulrich, "Deep reinforcement learning for spacecraft proximity operations guidance," *Journal of Spacecraft and Rockets*, Vol. 58, 2021, pp. 254–264, 10.2514/1.A34838.

[9] R. Furfaro, A. Scorsoglio, R. Linares, and M. Massari, "Adaptive generalized ZEM-ZEV feedback guidance for planetary landing via a deep reinforcement learning approach," *Acta Astronautica*, Vol. 171, 6 2020, pp. 156–171, 10.1016/j.actaastro.2020.02.051.

[10] S. V. Khoroshylov and C. Wang, "SPACECRAFT RELATIVE ON-OFF CONTROL VIA REINFORCEMENT LEARNING," *Space Science and Technology*, Vol. 30, 2024, pp. 3–14, 10.15407/knit2024.02.003.

[11] R. Furfaro, D. Cersosimo, and D. R. Wibben, "Asteroid precision landing via multiple sliding surfaces guidance techniques," *Journal of Guidance, Control, and Dynamics*, Vol. 36, 2013, pp. 1075–1092, 10.2514/1.58246.

[12] E. Capello, E. Punta, F. Dabbene, G. Guglieri, and R. Tempo, "Sliding-mode control strategies for rendezvous and docking maneuvers," *Journal of Guidance, Control, and Dynamics*, Vol. 40, 2017, pp. 1481–1488, 10.2514/1.G001882.

[13] Y. Shtessel, C. Edwards, L. Fridman, and A. Levant, *Sliding Mode Control and Observation*. Springer, 2014.

[14] Q. Li, B. Zhang, J. Yuan, and H. Wang, "Potential function based robust safety control for spacecraft rendezvous and proximity operations under path constraint," *Advances in Space Research*, Vol. 62, 11 2018, pp. 2586–2598, 10.1016/j.asr.2018.08.003.

[15] X. Li, Z. Zhu, and S. Song, "Non-cooperative autonomous rendezvous and docking using artificial potentials and sliding mode control," *Proceedings of the Institution of Mechanical Engineers, Part G: Journal of Aerospace Engineering*, Vol. 233, 3 2019, pp. 1171–1184, 10.1177/0954410017748988.

[16] X. Zhao and S. Zhang, "Adaptive saturated control for spacecraft rendezvous and docking under motion constraints," *Aerospace Science and Technology*, Vol. 114, 7 2021, 10.1016/j.ast.2021.106739.

[17] Y. Guo, D. Zhang, A. j. Li, S. Song, C. q. Wang, and Z. Liu, "Finite-time control for autonomous rendezvous and docking under safe constraint," *Aerospace Science and Technology*, Vol. 109, 2 2021. -sliding mode finite-time stable surface to deal with collision avoidance + APF.-ELLIPTICAL ORBIT, 10.1016/j.ast.2020.106380.

[18] L. Feng, Q. Ni, Y. Bai, X. Chen, and Y. Zhao, "Optimal sliding mode control for spacecraft rendezvous with collision avoidance," *2016 IEEE Congress on Evolutionary Computation, CEC 2016*, Institute of Electrical and Electronics Engineers Inc., 11 2016, pp. 2661–2668, 10.1109/CEC.2016.7744122.

[19] H. D. Curtis, *Orbital Mechanics for Engineering Students*. Elsevier, 2014.